# Effect of secondary decay on isoscaling: Results from the canonical thermodynamical model

Gargi Chaudhuri and Swagata Mallik

*Variable Energy Cyclotron Centre, 1/AF Bidhannagar, Kolkata 700064*

(Dated: July 14, 2010)



## Abstract

The projectile fragmentation reactions using $^{58}Ni$ & $^{64}Ni$ beams at 140 MeV/n on targets $^{9}Be$ & $^{181}Ta$ are studied using the canonical thermodynamical model coupled with an evaporation code. The isoscaling property of the fragments produced is studied using both the primary and the secondary fragments and it is observed that the secondary fragments also respect isoscaling though the isoscaling parameters $\alpha$ and $\beta$ changes. The temperature needed to reproduce experimental data with the secondary fragments is less than that needed with the primary ones. The canonical model coupled with the evaporation code successfully explains the experimental data for isoscaling for the projectile fragmentation reactions.

PACS numbers: 25.70Mn, 25.70Pq

## I. INTRODUCTION

Projectile fragmentation reaction is used extensively to study the reaction mechanisms in heavy ion collisions at intermediate and high energies. This is also an important technique for the production of rare isotope beams and is used by many radioactive ion beam facilities around the world. The fragment cross sections of projectile fragmentation reactions using primary beams of $^{40}Ca$, $^{48}Ca$, $^{58}Ni$ and $^{64}Ni$ at 140 MeV/nucleon on $^{9}Be$ and $^{181}Ta$ targets have been measured at the National Superconducting Cyclotron Laboratory at Michigan State University[1]. The canonical thermodynamical model(CTM)[2] has been used to calculate some of these fragment cross sections[3]. In the present work, an evaporation code has been developed and has been coupled with the canonical thermodynamical model. CTM coupled with this secondary decay code is then used to analyze the isoscaling data from the projectile fragmentation reactions. The lighter fragments produced from these reactions exhibit the linear isoscaling[4–6] phenomena and our model calculation also strongly supports this observation. The secondary fragments (produced after applying the evaporation code on the canonical model) also exhibit isoscaling like the primary fragments from the fragmentation reaction[7] but the temperature needed to reproduce the experimental data with the secondary fragments is lower than that required by the calculation with the primary fragments. The isoscaling parameters $\alpha$ and $\beta$ as obtained in the present work from the model calculations agree closely with those obtained from the experimental data. These parameters as obtained from the secondary fragments are lower in magnitude than those obtained from the primary ones. This effect is also seen in the dynamical models [8] though the reduction is much more there. The isoscaling behaviour displayed by the fragments produced in the projectile fragmentation reactions and the effect of evaporation on it in the framework of the HIPSE model has been discussed recently in [9].

This paper is structured as follows. First we describe the canonical model briefly in Sec.II. In the same section we also present the main features of the evaporation code which is used to calculate the secondary fragments. In Sec.III we present the results. The effect of sequential decay on the distribution of the isotopic fragments is discussed. The isoscaling phenomena as displayed by the primary as well as the secondary fragments is also described in this section and are compared with the experimental data. In Sec. IV we present the summary.

## II. THE STATISTICAL MODEL

In models of statistical disassembly of a nuclear system formed by the collision of two heavy ions at intermediate energy one assumes that because of multiple nucleon-nucleon collisions a statistical equilibrium is reached. Consequently, the temperature rises. The system expands from normal density and composites are formed on the way to disassembly. As the system reaches between three to six times the normal volume, the interactions between composites become unimportant (except for the long range Coulomb interaction) and one can do a statistical equilibrium calculation to obtain the yields of composites at a volume called the freeze-out volume. The partitioning into available channels can be solved in the canonical ensemble where the number of particles in the nuclear system is finite (as it would be in experiments). In the next subsection we describe the canonical model.

### A. The canonical thermodynamical model

In this section we describe briefly the canonical thermodynamical model. Assume that the system with $A_0$ nucleons and $Z_0$ protons at temperature $T$, has expanded to a higher than normal volume and the partitioning into different composites can be calculated according to the rules of equilibrium statistical mechanics. In a canonical model, the partitioning is done such that all partitions have the correct $A_0, Z_0$ (equivalently $N_0, Z_0$). Details of the implementation of the canonical model can be found elsewhere [2]; here we give the essentials necessary to follow the present work.

The canonical partition function is given by

$$Q_{N_0,Z_0} = \sum \prod \frac{\omega_{I,J}^{n_{I,J}}}{n_{I,J}!} \tag{1}$$

Here the sum is over all possible channels of break-up (the number of such channels is enormous) which satisfy $N_0 = \sum I \times n_{I,J}$ and $Z_0 = \sum J \times n_{I,J}$; $\omega_{I,J}$ is the partition function of one composite with neutron number $I$ and proton number $J$ respectively and $n_{I,J}$ is the number of this composite in the given channel. The one-body partition function $\omega_{I,J}$ is a product of two parts: one arising from the translational motion of the composite and another from the intrinsic partition function of the composite:

$$\omega_{I,J} = \frac{V_f}{h^3}(2\pi mT)^{3/2}A^{3/2} \times z_{I,J}(int) \tag{2}$$

Here $A = I + J$ is the mass number of the composite and $V_f$ is the volume available for translational motion; $V_f$ will be less than $V$, the volume to which the system has expanded at break up. We use $V_f = V - V_0$ , where $V_0$ is the normal volume of nucleus with $Z_0$ protons and $N_0$ neutrons. In this calculation we have used a fairly typical value $V = 6V_0$.

The probability of a given channel $P(\vec{n}_{I,J}) \equiv P(n_{0,1}, n_{1,0}, n_{1,1}.....n_{I,J}.....)$ is given by

$$P(\vec{n}_{I,J}) = \frac{1}{Q_{N_0,Z_0}} \prod \frac{\omega_{I,J}^{n_{I,J}}}{n_{I,J}!} \tag{3}$$

The average number of composites with $I$ neutrons and $J$ protons is seen easily from the above equation to be

$$\langle n_{I,J} \rangle = \omega_{I,J} \frac{Q_{N_0-I,Z_0-J}}{Q_{N_0,Z_0}} \tag{4}$$

The constraints $N_0 = \sum I \times n_{I,J}$ and $Z_0 = \sum J \times n_{I,J}$ can be used to obtain different looking but equivalent recursion relations for partition functions[10]. For example

$$Q_{N_0,Z_0} = \frac{1}{N_0} \sum_{I,J} I \omega_{I,J} Q_{N_0-I,Z_0-J} \tag{5}$$

These recursion relations allow one to calculate $Q_{N_0,Z_0}$

We list now the properties of the composites used in this work. The proton and the neutron are fundamental building blocks thus $z_{1,0}(int) = z_{0,1}(int) = 2$ where 2 takes care of the spin degeneracy. For deuteron, triton, $^3$He and $^4$He we use $z_{I,J}(int) = (2s_{I,J} + 1)\exp(-\beta E_{I,J}(gr))$ where $\beta = 1/T, E_{I,J}(gr)$ is the ground state energy of the composite and $(2s_{I,J} + 1)$ is the experimental spin degeneracy of the ground state. Excited states for these very low mass nuclei are not included. For mass number $A = 5$ and greater we use the liquid-drop formula. For nuclei in isolation, this reads ($A = I + J$)

$$z_{I,J}(int) = \exp \frac{1}{T}[W_0 A - \sigma(T) A^{2/3} - \kappa \frac{J^2}{A^{1/3}} - C_s \frac{(I-J)^2}{A} + \frac{T^2 A}{\epsilon_0}] \tag{6}$$

The derivation of this equation is given in several places [2, 11] so we will not repeat the arguments here. The expression includes the volume energy, the temperature dependent surface energy, the Coulomb energy and the symmetry energy. The term $\frac{T^2 A}{\epsilon_0}$ represents contribution from excited states since the composites are at a non-zero temperature.

We also have to state which nuclei are included in computing $Q_{N_0,Z_0}$ (eq.(17)). For $I, J$, (the neutron and the proton number) we include a ridge along the line of stability. The

liquid-drop formula above also gives neutron and proton drip lines and the results shown here include all nuclei within the boundaries.

The long range Coulomb interaction between different composites can be included in an approximation called the Wigner-Seitz approximation. We incorporate this following the scheme set up in [11].

### B. The evaporation code

The statistical multifragmentation model described above calculates the properties of the collision averaged system that can be approximated by an equilibrium ensemble. Ideally, one would like to measure the properties of excited primary fragments after emission in order to extract information about the collisions and compare directly with the equilibrium predictions of the model. However, the time scale of a nuclear reaction($10^{-20}s$) is much shorter than the time scale for particle detection ($10^{-9}s$). Before reaching the detectors, most fragments decay to stable isotopes in their ground states. Thus before any model simulations can be compared to experimental data, it is indispensable to have a model that simulates sequential decays. A Monte Carlo technique is employed to follow all decay chains until the resulting products are unable to undergo further decay. For the purposes of the sequential decay calculations the excited primary fragments generated by the statistical model calculations are taken as the compound nucleus input to the evaporation code. Hence, every primary fragment is decayed as a separate event.

We consider the deexcitation of a primary fragment of mass $A$, charge $Z$ and temperature $T$. The succseesive particle emission from the hot primary fragments is assumed to be the basic deexcitation mechanism. For each event of the primary breakup simulation, the entire chain of evaporation and secondary breakup events is Monte Carlo simulated. The standard Weisskopf evaporation scheme is used to take into account evaporation of nucleons, $d$, $t$, $He^3$ and $\alpha$. The decays of particle stable excited states via gamma rays were also taken into account for the sequential decay process and for the calculation of the final ground state yields. We have also considered fission as a deexcitation channel though for the nuclei of mass $< 100$ its role will be quite insignificant. The process of light particle emission from a compound nucleus is governed by the emission width $\Gamma_\nu$ at which a particle of type $\nu$ is emitted. According to Weisskopf's conventional evaporation theory [12], the partial decay

width for emission of a light particle of type $\nu$ is given by

$$\Gamma_\nu = \frac{gm\sigma_0}{\pi^2\hbar^2}\frac{(E^* - E_0 - V_\nu)}{a_R}\exp(2\sqrt{a_R(E^* - E_0 - V_\nu)} - 2\sqrt{a_P E^*}) \tag{7}$$

Here $m$ is the mass of the emitted particle, $g$ is its spin degeneracy. $E_0$ is the particle separation energy which is calculated from the binding energies of the parent nucleus, daughter nucleus and the binding energy of the emitted particle and the liquid drop model is used to calculate the binding energies. The subscript $\nu$ refers to the emitted particle, $P$ refers to the parent nuclei and $R$ refers to the residual(daughter) nuclei. $a_P$ & $a_R$ are the level density parameters of the parent and residual nucleus respectively. The level density parameter is given by $a = A/16MeV^{-1}$ and it connects the excitation energy $E^*$ and temperature $T$ through the following relations.

$$\begin{aligned} E^* &= a_P T_P^2 \\ (E^* - E_0 - V_\nu) &= a_R T_R^2. \end{aligned} \tag{8}$$

where $T_P$ & $T_R$ are the temperatures of the emitting(parent) and the final(residual) nucleus respectively. $V_\nu$ is the Coulomb barrier which is zero for neutral particles and non-zero for charged particles. In order to calculate the Coulomb barrier for charged particles of mass $A \geq 2$ we use a touching sphere approximation[13],

$$\begin{aligned} V_\nu &= \frac{Z_\nu(Z_P - Z_\nu)e^2}{r_i\{A_\nu^{1/3} + (A_P - A_\nu)^{1/3}\}} \qquad \text{for} \qquad A_\nu \geq 2 \\ &= \frac{(Z_P - 1)e^2}{r_i A_P^{1/3}} \qquad \text{for} \qquad protons \end{aligned} \tag{9}$$

where $r_i$ is taken as 1.44m.

$\sigma_0$ is the geometrical crosssection (inverse cross section) associated with the formation of the compound nucleus(parent) from the emitted particle and the daughter nucleus and is given by $\sigma_0 = \pi R^2$ where,

$$\begin{aligned} R &= r_0\{(A_P - A_\nu)^{1/3} + {A_\nu}^{1/3}\} \qquad \text{for} \quad A_\nu \geq 2 \\ &= r_0(A_P - 1)^{1/3} \qquad \text{for} \quad A_\nu = 1. \end{aligned} \tag{10}$$

where $r_0 = 1.2$ fm.

For the emission of giant dipole $\gamma$-quanta we take the formula given by Lynn[14]

$$\Gamma_\gamma = \frac{3}{\rho_P(E^*)} \int_0^{E^*} d\varepsilon \rho_R(E^* - \varepsilon) f(\varepsilon) \tag{11}$$

with

$$f(\varepsilon) = \frac{4}{3\pi} \frac{1+\kappa}{m_n c^2} \frac{e^2}{\hbar c} \frac{N_P Z_P}{A_P} \frac{\Gamma_G \varepsilon^4}{(\Gamma_G \varepsilon)^2 + (\varepsilon^2 - E_G^2)^2} \tag{12}$$

with $\kappa = 0.75$, and $E_G$ and $\Gamma_G$ are the position and width of the giant dipole resonance.

For the fission width we have used the simplified formula of Bohr-Wheeler given by

$$\Gamma_f = \frac{T_P}{2\pi} \exp\left(-B_f/T_P\right) \tag{13}$$

where $B_f$ is the fission barrier of the compound nucleus given by[15]

$$B_f(MeV) = -1.40 Z_P + 0.22(A_P - Z_P) + 101.5. \tag{14}$$

Once the emission widths are known, it is required to establish the emission algorithm which decides whether a particle is being emitted from the compound nucleus. This is done [16] by first calculating the ratio $x = \tau/\tau_{tot}$ where $\tau_{tot} = \hbar/\Gamma_{tot}$, $\Gamma_{tot} = \sum_\nu \Gamma_\nu$ and $\nu = n, p, d, t, He^3, \alpha, \gamma$ or fission and then performing Monte-Carlo sampling from a uniformly distributed set of random numbers. In the case that a particle is emitted, the type of the emitted particle is next decided by a Monte Carlo selection with the weights $\Gamma_\nu/\Gamma_{tot}$ (partial widths). The energy of the emitted particle is then obtained by another Monte Carlo sampling of its energy spectrum. The energy, mass and charge of the nucleus is adjusted after each emission. This procedure is followed for each of the primary fragment produced at a fixed temperature and then repeated over a large ensemble and the observables are calculated from the ensemble averages. . The number and type of particles emitted and the final decay product in each event is registered and are taken into account properly keeping in mind the overall charge and baryon number conservation.

## III. RESULTS

First we will show our calculations for $^{58}Ni$ on $^{9}Be$ reaction and $^{64}Ni$ on $^{9}Be$ reaction. In the model, the target imparts a certain amount of energy to the projectile transforming it to

a projectile like fragment(PLF) with a temperature. This excited PLF will then expand and form composites during the expansion. The partioning of the PLF into different composites is done by the rules of equilibrium statistical mechanics in a freeze-out volume. We consider production of different isotopes from the statistical breakup of the dissociating system. If $< n_{i,j} >$ is the average number(multiplicity) of composites with $i$ neutrons and $j$ protons, then the cross-section for this composite is $\sigma(i,j) = C < n_{i,j} >$, where C is a constant not calculable from the thermodynamic model. It depends upon the dynamics that are outside the scope of this model. To be able to compute $< n_{i,j} >$ we need to know the mass and charge of the PLF and its temperature. The source sizes adopted for this calculation are zero order guesses. It could be sometimes smaller or greater depending on the diffusion from the target. For $^{64}Ni$ or $^{58}Ni$ on $^{9}Be$ which is a small target the choice of the mass and the charge of the PLF is limited. It can be slightly less than that of the projectile to as large as that of the projectile plus $^{9}Be$, the last being the case when the much larger projectile swallows the small target and drags it along retaining PLF features. Similarly we have some limits on energy imparted(this fixes the temperature). This energy can be small or upto the upper limit. The upper limit is given by the case of projectile swallowing Be and all the energy transforming into internal excitation(no part going into collective flow). In the canonical calculation, the dissociating system is taken to be $^{58}Ni +^{9} Be(N_0 = 35, Z_0 = 32)$ and for the other reaction the dissociating system is taken to be $^{64}Ni +^{9} Be(N_0 = 41, Z_0 = 32)$.All composites between drip lines are included as detailed in Sec.IIA with the highest values of N, Z terminating at $N_0$, $Z_0$. The temperature is taken to be 5.8 MeV for both the reactions.

Fig. 1 displays the isotopic distribution for Z=12(magnesium) produced from both the the reactions. The dashed lines correspond to the distributions of the primary fragments while the solid lines correspond to the distributions after sequential decay. As expected, the more neutron rich system with $N_0/Z_0 = 1.28$ (right panel) produces more neutron rich isotopes than the neutron deficient system with $N_0/Z_0 = 1.09$ (left panel). In all cases, the primary distributions are much wider and more neutron rich than the final distributions. The peak positions of the isotopic distributions of both the primary and the secondary fragments coincide in case of the neutron deficient system as seen from the left panel of the figure. In case of the neutron rich system(right panel) the peak of the distribution of the secondary fragments has shifted to the left with respect to that of the primary. The experimental isotopic distributions(solid squares with error bars) agree much more with the

final results obtained after secondary decay than with the primary distributions. The width and peak position of the isotopic distribution after the secondary decay agrees very well with the experimental data. The model also successfully reproduces the rapid fall in crosssection for large neutron number.

We will now discuss the results about isoscaling. It is observed from the experimental data[17] that the light fragments emitted from the $^{58}Ni$ and $^{64}Ni$ systems exhibit the linear isoscaling behaviour represented by the equation

$$R_{21} = Y_2(N,Z)/Y_1(N,Z) = C\exp(\alpha N + \beta Z). \tag{15}$$

where the isoscaling ratio $R_{21}(N,Z)$ is factored into two fugacity terms $\alpha$ and $\beta$, which contain the differences of the chemical potentials for neutrons and protons of the two reaction systems. $Y_2(N,Z)$ refers to the yield of fragment(N,Z) from system 2 which is usually taken to be the neutron-rich one and $Y_1(N,Z)$ refers to the same from system 1. C is a normalization factor of the isoscaling ratio. It is observed from our model that both the primary as well as the secondary fragments exhibit isoscaling. Fig. 2 shows the isoscaling results for Ni on Be system for the primary fragments. The ratio $R_{21}$ is plotted as function of the neutron number from Z =6 to Z= 13 in the left panel whereas the right panel displays the ratio as function of the proton number Z from N=8 to N=15. It is seen that the primary fragments exhibit very well the linear isoscaling behaviour for the lighter fragments over a wide range of isotopes and isotones. The lines in the figures are the best fits of the calculated $R_{21}$ ratios(open triangles) to Eq.15. They are essentially linear and parallel on the semi log plot .

Fig. 3 displays the isoscaling results for the secondary fragments. The open triangles are the results obatined from our model while the solid squares with the error bars are the experimental ratios. We have shown the isoscaling results for the even Z and odd Z isotopes in two separate panels for the sake of clarity. While comparing with the results of the primary fragments in Fig 2, it is evident that the isoscaling is valid for a limited range of isotopes for the secondary fragments as compared to the primary ones. When the isotopes away from the valley of stable nuclei are considered, the trends for the secondary fragments are not as clearly consistent with the isoscaling law as are the trends of the primary distribution. One can conclude from this that isoscaling is approximately valid in the case of the secondary fragments. The lines in the figures are the best fits of the calculated $R_{21}$ ratios which agree

closely with the experimental data. The temperature required to reproduce isoscaling data with the primary fragments is about 8 MeV[7] whereas that required for the secondary fragments is 5.8 MeV. This decrease was already predicted in one of our earlier papers[7] in Sec.9. It has also been found out by Ono et al.[8] that the effect of secondary decay is to decrease the isoscaling parameter $\alpha$ by about 50%. This is indeed what emerges from our calculations after including secondary decay code with the canonical model though the amount of reduction is less as compared to the dynamical model. Tha value of $\alpha$ as obtained from the fits of the primary fragments (left panel of Fig. 2) is 0.713 whereas that obtained from the secondary fragments is 0.580 which is much closer to the experimentally obtained value for $\alpha$[17] equal to 0.566.

In Fig. 4 we have also plotted the isoscaling ratios for different neutron number values as function of the proton number Z and thereby calculated the other isoscaling parameter $\beta$ from them. The value of $\beta$ as obatined from the linear fits of the primary fragments( right panel of Fig. 2) is -0.849. For the secondary fragments, the value of $\beta$ from our model is -0.634 whereas the experimentally obtained value is -0.621. The value of $\beta$ also decreases in the case of secondary from the primary ones as in the case of $\alpha$. The results obtained after the sequential decay matches very well with the experimental ratios. As for the isotopes in Fig 3, for the isotones also it is seen that the linear isoscaling is valid for a limited range in case of secondary fragments as compared to the primary ones(right panel of Fig.2).

We now turn to the case where the target is $^{181}Ta$. One can consider the extreme limit which is target independence and by which we mean that $N_0$, $Z_0$ refers to simply to the case where just the projectile is the disintegrating system. The more likely scenario where some matter has diffused to or from the target has many possibilities. In principle, the target could shear away some material from the projectile leaving a PLF which is a fraction of the projectile. For a peripheral collision this is less likely than the alternative of the projectile picking up part of nuclear matter from the tail region of the much larger target. The amount of nuclear matter curved out of Ta will be small(for the disintegrating system to retain PLF characteristics) but other than that not much can be said and an integration over the different possibilities might be essential. Keeping this limitation in mind, we compared with different possible scenarios and the case with projectile plus 10 neutrons and 8 protons from the target, i.e, projectile $+^{18}0$ yielded the best results. It is also seen that target independence gives worse results than this case. The agreement of our model calculations

with experimental data is pretty good in this case. The temperature used for this reaction is 6.2 MeV.

Fig. 5 and Fig. 6 are similar to Fig. 3 & Fig. 4 except for the fact that they are for the case where the target is $^{181}Ta$ instead of $^{9}Be$. The theoretical slope $\alpha$ as obtained from Fig. 5 from the fit of the secondary fragments is 0.459 while the experimentally obtained slope is 0.432. The straight line fit to the calculated points matches nicely with the experimental ratios. The value of $\beta$ as obtained from our model from the slopes in Fig. 6 is -0.489 whereas the experimentally obtained value is -0.487. Thus we find that the values of the isoscaling parametrs as obtained from the secondary fragments for both the targets agree quite well with the experimental values as can be seen from Table 1.

| Target material | Isoscaling parameters | primary | secondary | experiment |
|---|---|---|---|---|
| $^{9}Be$ | $\alpha$ $(Z_{min} = 6, Z_{max} = 13)$ | 0.713 | 0.580 | 0.566 |
| $^{9}Be$ | $\beta$ $(N_{min} = 8, N_{max} = 15)$ | -0.849 | -0.634 | -0.621 |
| $^{181}Ta$ | $\alpha(Z_{min} = 6, Z_{max} = 13)$ | 0.619 | 0.459 | 0.432 |
| $^{181}Ta$ | $\beta$ $N_{min} = 8, N_{max} = 15)$ | -0.682 | -0.489 | -0.487 |

TABLE I: Best fit values of the isoscaling parametrs $\alpha$ and $\beta$ for the two targets $^{9}Be$ and $^{181}Ta$. The values obtained from the slope of the primary and secondary fragments as well as the experimental values are tabulated. In the second column the range of $Z$ or $N$ values used to calculate the parameters are indicated.

## IV. SUMMARY

This work deals with the developing of the sequential decay code and successfully coupling it with the canonical thermodynamical model in order to compare the properties of the secondary fragments with the experimental data. The width, peak position and rapid fall in cross-section of the isotopic distribution of the secondary fragments matches well with the experimental data. The main purpose is to examine the effects of sequential decay on the phenomenon of isoscaling. The secondary fragments also shows isoscsling and the the isoscaling parameters calculated from the secondary fragments matches closely with the experimental data. The temperature required to reproduce the experimental data with the

secondary fragments is less than needed by the primary ones. We finally conclude that the canonical thermodynamical model can explain the isoscaling properties of the lighter fragments produced in the projectile fragmentation reaction.

## V. ACKNOWLEDGEMENT

The authors gratefully acknowledges important discussions with Prof. Subal Dasgupta. They are thankful to Prof. M.B. Tsang and Dr. M. Mocko. Valuable suggestions from Dr. Santanu Pal and Jhilam Sadhukhan is also acknowledged gratefully.

[1] M. Mocko et al., Phys. Rev C**74**, 054612 (2006)

[2] C. B. Das, S. Das Gupta, W. G. Lynch, A. Z. Mekjian, and M. B. Tsang, Phys. Rep **406**, 1, (2005).

[3] G. Chaudhuri, S. Das Gupta, W. G. Lynch, M. Mocko and M.B. Tsang, Phys. Rev. C**76** 067601 (2007).

[4] H. S. Xu et al., Phys. Rev. Lett. **85**, 716, (2000).

[5] M. B. Tsang, W. A. Friedman, C. K. Gelbke, W. G. Lynch, G. Verde, and H. S. Xu, Phys. Rev. Lett. **86**, 5023 (2001).

[6] M. B. Tsang et al., Phys. Rev C**64**, 054615 (2001).

[7] G. Chaudhuri, S. Das Gupta and M. Mocko, Nucl. Phys. A**813**, 293-313 (2008).

[8] A. Ono et al.,arxiv:nucl-ex/0507018v2.

[9] Y. Fu, D.Q. Fang, Y.G. Ma, X.Z. Cai, X.Y. Sun and W.D. Tian, Nucl. Phys. A**834**, 584c (2010).

[10] K.C. Chase and A. Z. Mekjian, Phys. Rev. C**52**, R2339(1995).

[11] J. P. Bondorf, A. S. Botvina, A. S. Iljinov, I. N. Mishustin and K. Sneppen, Phys. Rep. **257**, 133 (1995).

[12] V. Weiskoff, Phys. Rev. **52**, 295(1937).

[13] W.A. Friedman and W. G. Lynch, Phys. Rev C**28**, 16 (1983).

[14] J. E. Lynn, *Theory of Neutron Resonance Reactions*,Clarendon, Oxford, 1968, p-325.

[15] C. Guaraldo, V. Lucherini, E. D. Sanctis, A.S. Iljinov, M. V. Mebel and S. Lo Nigro, Nuovo Cimento **103A**, 4 (1990).

[16] G. Chaudhuri, PhD thesis(Chapter IV), arXiv:nucl-th/0411005

[17] M. Mocko, PhD thesis, Michigan State University 2006.

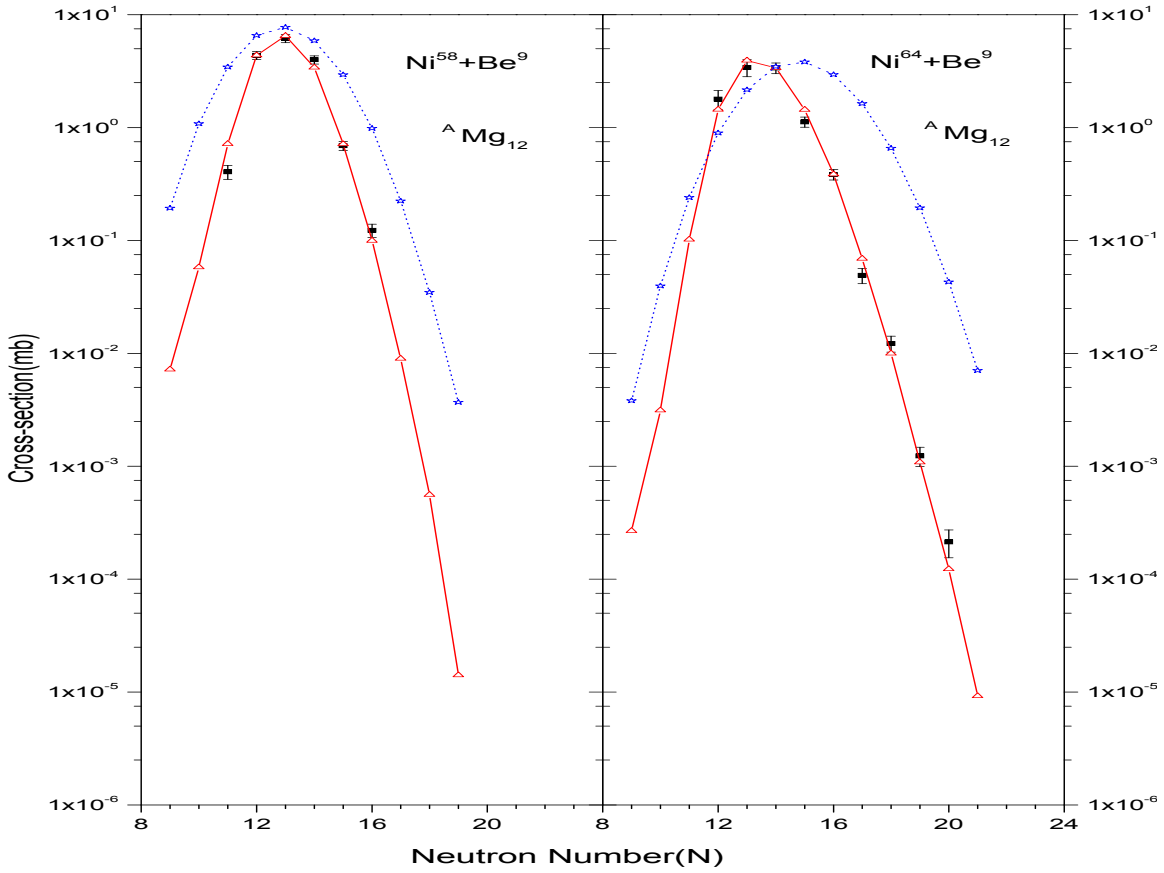


FIG. 1: Experimental cross sections of magnesium isotopes(squares with error bars) compared with theoretical results: primary fragments( open stars joined by dotted line) and secondary fragments(open triangles joined by solid line). The left panel is for the reaction $^{58}$Ni on $^{9}$Be while the right panel is for $^{64}$Ni on $^{9}$Be reaction. The temperature is 5.8 MeV for both the reactions.

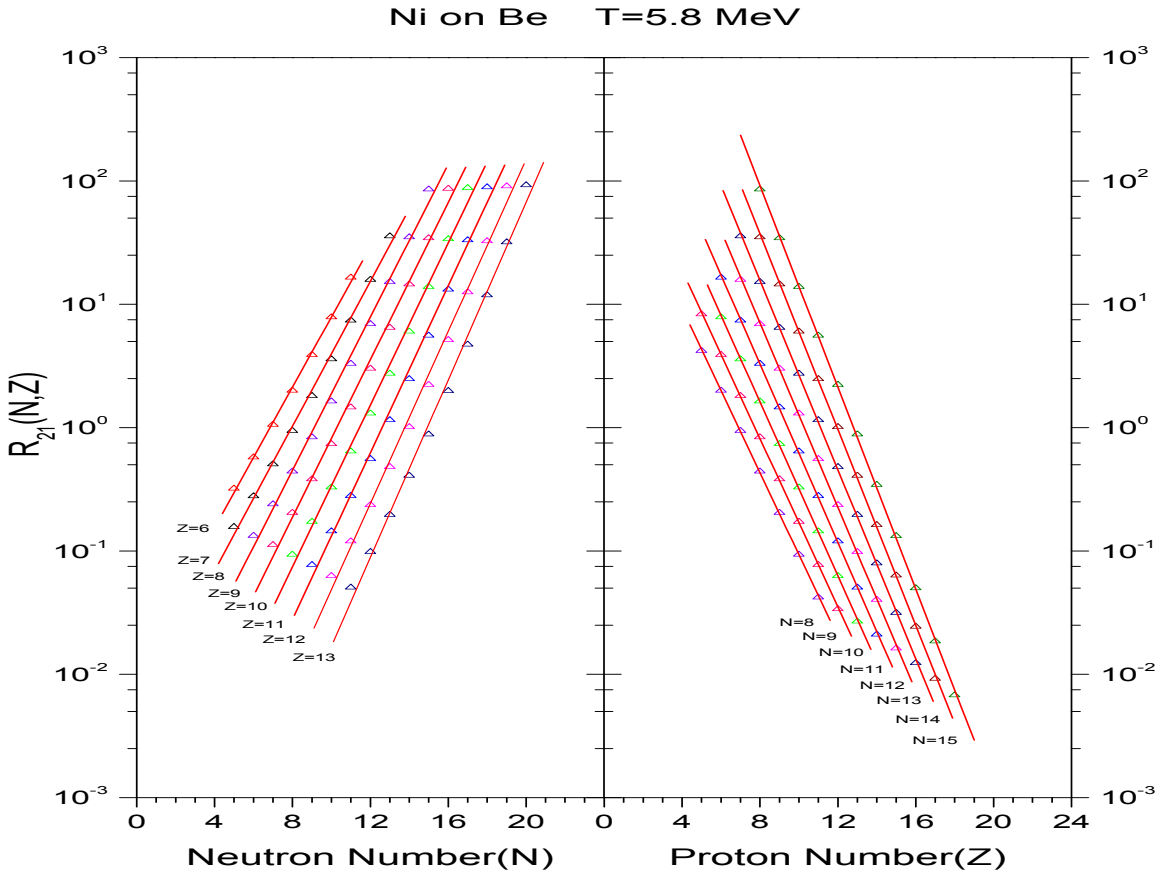


FIG. 2: Ratios($R_{21}$) of multiplicities of primary fragments of producing the nucleus $(N, Z)$ where reaction 1 is $^{58}$Ni on $^{9}$Be and reaction 2 is $^{64}$Ni on $^{9}$Be. The left panel shows the ratios as function of neutron number $N$ for fixed $Z$ values from 6 to 13, while the right panel displays the ratios as function of proton number $Z$ for fixed neutron numbers from $N = 8$ to 15. The lines drawn through the theoretical points(open triangles) are best fits of the calculated ratios. The temperature used for both the reacions is 5.8 MeV.

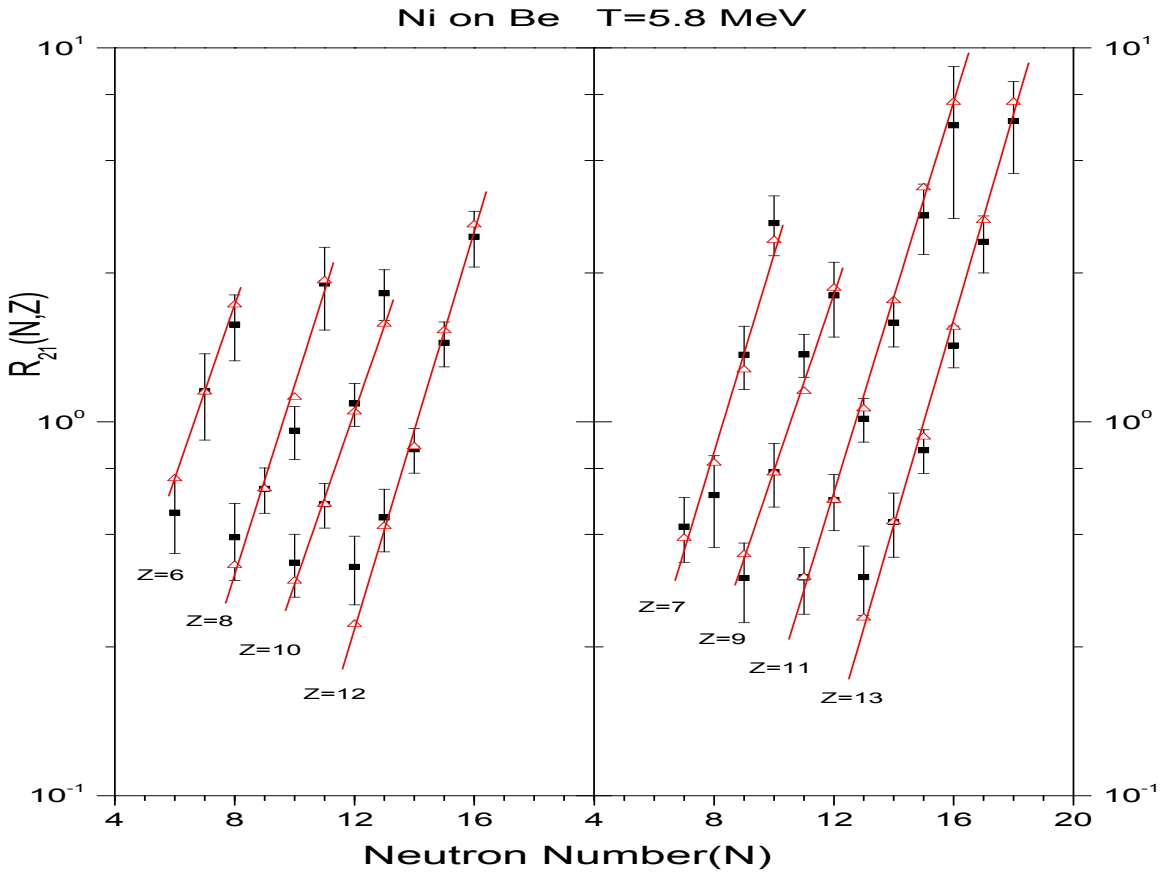


FIG. 3: Ratio of multiplicities of the secondary fragments of producing the nucleus $(N, Z)$ where reaction 1 is $^{58}$Ni on $^{9}$Be and reaction 2 is $^{64}$Ni on $^{9}$Be compred with the ratios of the experimental cross sections of the same two reactions. The left panel shows the even $Z$ isotopes while the right panel shows the results for the odd ones. The lines drawn through the theoretical points(open triangles) are best fits of the calculated ratios. The experimental points are shown by solid squares with error bars.The temperature used for both the reacions is 5.8 MeV.

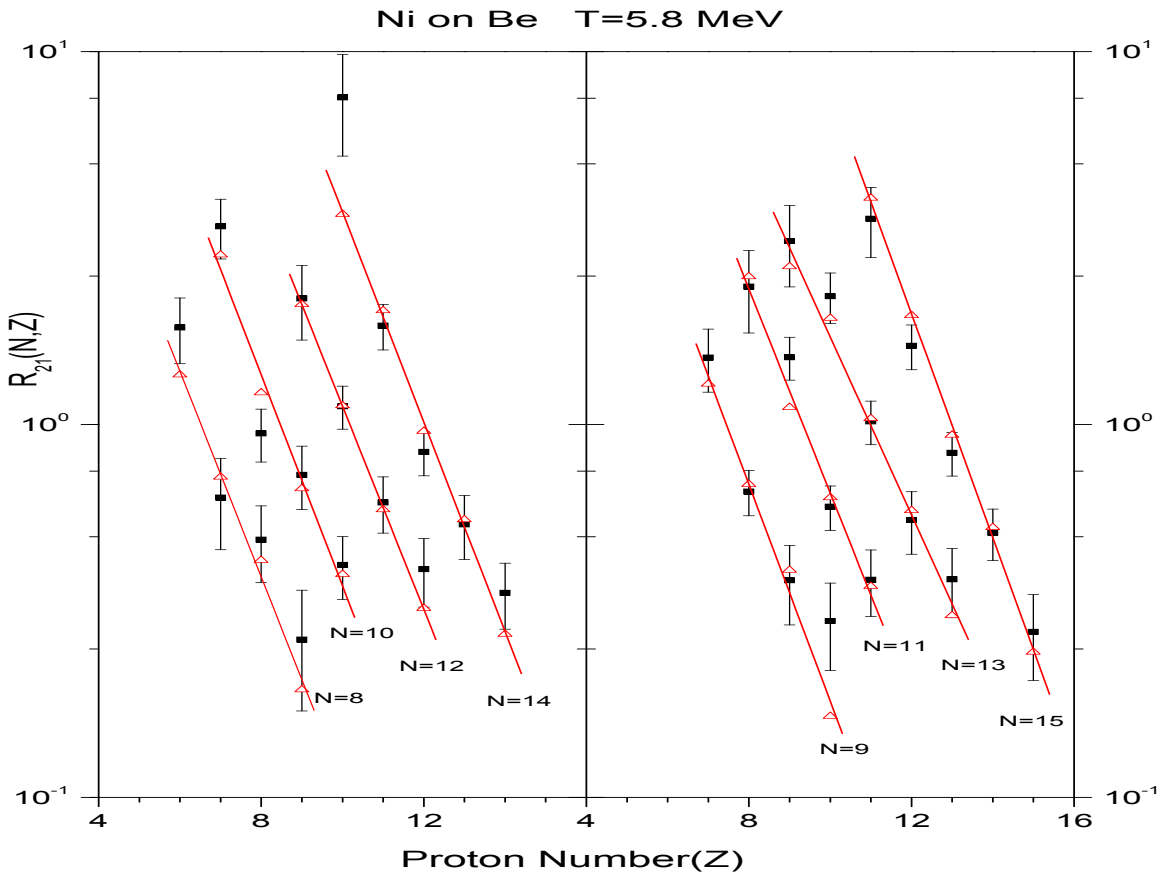


FIG. 4: Same as Fig. 3 except that the ratios are plotted as function of the proton number $Z$ for fixed neutron numbers. The left panel shows the results for the even neutron numbers while the right ones show those for the odd ones.

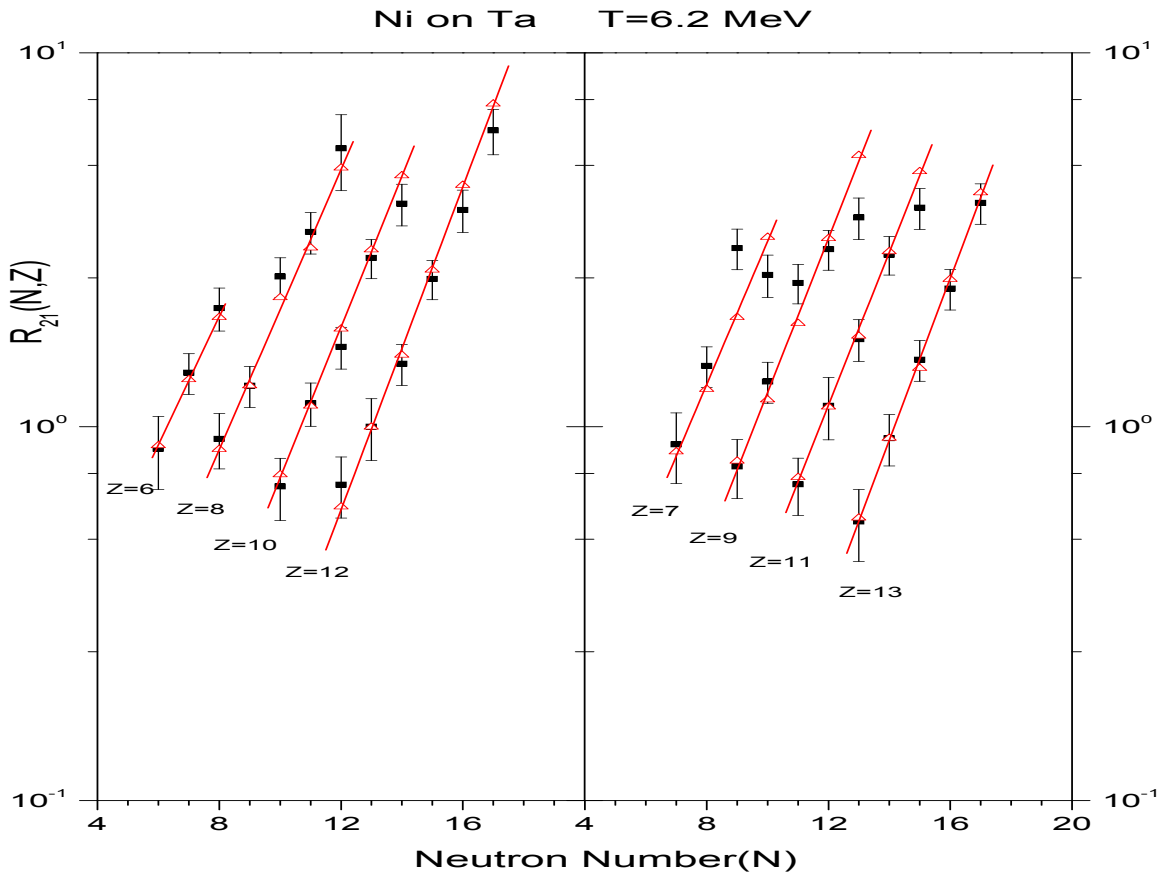


FIG. 5: Same as Fig. 3 except that here the target is $^{181}Ta$ instead of $^{9}Be$. The temperature used for both the the reactions is 6.2 MeV.

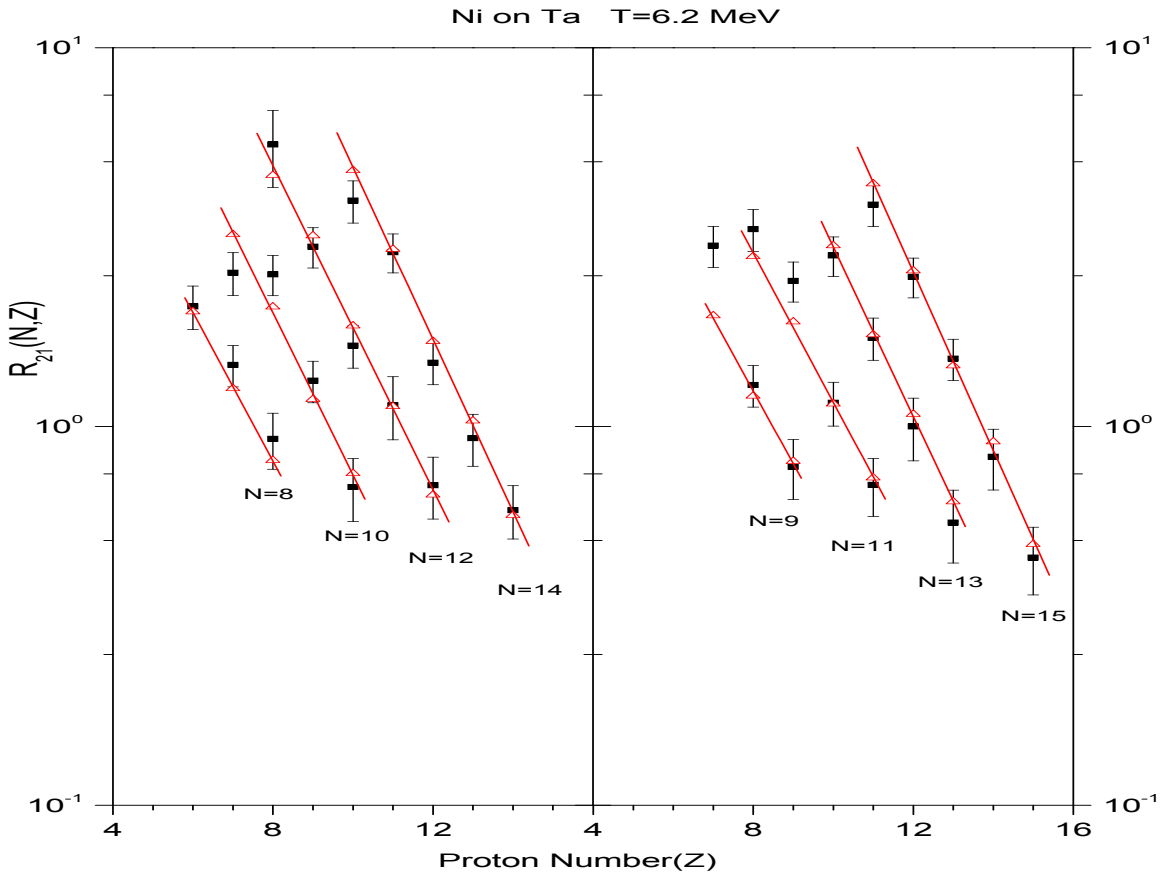


FIG. 6: Same as Fig. 4 except that here the target is $^{181}Ta$ instead of $^{9}Be$. The temperature used for both the reactions is 6.2 MeV.